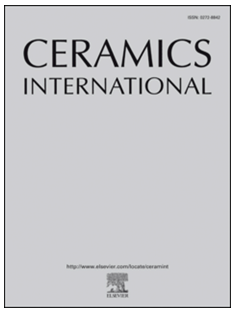

Reduced graphene oxide-ZnO hybrid composites as photocatalysts: The role of nature of the molecular target in catalytic performance

Anton Landström, Alessandro Gradone, Raffaello Mazzaro, Vittorio Morandi, Isabella Concina

PII: S0272-8842(21)00964-0

DOI: https://doi.org/10.1016/j.ceramint.2021.03.271

Reference: CERI 28336

To appear in: *Ceramics International*

Received Date: 1 February 2021

Revised Date: 25 March 2021

Accepted Date: 26 March 2021

Please cite this article as: A. Landström, A. Gradone, R. Mazzaro, V. Morandi, I. Concina, Reduced graphene oxide-ZnO hybrid composites as photocatalysts: The role of nature of the molecular target in catalytic performance *Ceramics International*, https://doi.org/10.1016/j.ceramint.2021.03.271.

Reduced graphene oxide-ZnO hybrid composites as photocatalysts:

The role of nature of the molecular target in catalytic performance

Anton Landström[1], Alessandro Gradone[2,3], Raffaello Mazzaro[2],

Vittorio Morandi[2], Isabella Concina[1,*]

[1] Department of Engineering Sciences and Mathematics, Luleå University of Technology, 97187 Luleå, Sweden

[2]National research council, Institute for Microelectronics and Microsystems, Via Piero Gobetti 101, 40129, Bologna, Italy

[3]Department of Chemistry "G. Ciamician", University of Bologna, Via Francesco Selmi 2, 40126, Bologna, Italy

* Corresponding author: isabella.concina@ltu.se

Abstract

Spurred by controversial literature findings, we enwrapped reduced graphene oxide (rGO) in ZnO hierarchical microstructures (rGO loadings spanning from 0.01 to 2 wt%) using an *in situ* synthetic procedure. The obtained hybrid composites were carefully characterized, aiming at shining light on the possible role of rGO on the claimed increased performance as photocatalysts. Several characterization tools were exploited to unveil the effect exerted by rGO, including steady state and time resolved photoluminescence, electron microscopies and electrochemical techniques, in order to evaluate the physical, optical and electrical features involved in determining the catalytic degradation of rhodamine B and phenol in water.

Several properties of native ZnO structures were found changed upon the rGO enwrapping (including optical absorbance, concentration of native defects in the ZnO matrix and double-layer capacitance), which are all involved in determining the photocatalytic performance of the hybrid composites. The findings discussed in the present work highlight the high complexity of the field of application of graphene-derivatives as supporters of semiconducting metal oxides functionality, which has to be analyzed through a multi-parametric approach.

Keywords

- reduced graphene oxide

- zinc oxide

- photoluminescence

- crystalline defects

- photocatalysis

1. Introduction

Over the last decade an impressive attention has been dedicated to the synthesis and use in functional applications of graphene-semiconductor hybrid composites (GSHCs). [1] Among the functional applications, a prominent role is played by (photo)catalysis, where wide band gap n-type semiconductor metal oxides (MOx), like TiO_2, SnO_2 and ZnO are acknowledged as solid candidates to sustain useful chemical reactions.[2][3] The interest raised by these materials is not only due to their well-established catalytic skills, but also to the possibility to fabricate them at the nanoscale and integrate them in GSHCs. [4]

The first studies reporting the possibility of incorporating an n-type MOx semiconductor with graphene[5][6] highlighted the chance of synthesizing photoactive graphene-semiconductor composites and using graphene-based materials as mediators in photogenerated charge transport and storage. Incorporation of graphene, typically reduced graphene oxide (rGO), has been reported to enhance photocatalytic activity in common MOx such as iron oxide, [7] zinc oxide, [8–13] and titanium dioxide,[14–16] with graphene loading spanning within a wide range (0.1-75 wt%).

Most published studies in the field of GSHCs claim outstanding enhancement of functional performance, emphasizing the capability of graphene derivatives (like graphene oxide, GO, and reduced graphene oxide, rGO) of capturing charges photogenerated within the MOx, thus reducing the electron-hole recombination, known as possibly the heaviest limitation of MOx as functional materials.[17–19] However, the mechanisms behind the observed performance enhancement are still controversial and several limitations associated to the use of graphene derivatives combined with

semiconducting MOx have also been reported. Among these latter, a shielding effect exerted by graphene derivatives in relatively high amount has been often reported,[20] pointing out at the relevance of properly dosing the presence of carbon materials in catalytic composites, but not only. Similar issues have been highlighted also when composites of this kind were used in photovoltaics and supercapacitors.[21] In the specific field of catalysis, moreover, the beneficial role of graphene needs to be read in the light of the specific reaction mechanism[22] and the use of "lower quality" carbon-based materials has also been proved effective.

Among the claimed reasons behind the performance enhancement, it is worth mentioning the partial inhibition of direct exciton recombination (often inferred from the decreased intensity of near band edge emission in photoluminescence spectra),[23] good interfacial charge transfer between graphene and MOx [24] and enhanced light absorption.[25] However, improving the photocatalytic performance of a given material is not only a matter of harnessing and using useful charges, but also of modulating the presence of active reaction sites. Graphene derivatives, in combination with MOx, have been also sometimes reported as efficient adsorbents,[26] which can significantly contribute to the apparent rate constant in a photocatalytic reaction.

The topic of the appropriate amount of graphene derivatives to incorporate in the hybrid composites is as well a critical point in the synthesis and application of this class of materials: literature data present controversial information in this frame and almost nothing is known about the possible effect on the structure of the nano- and micro-structured MOx synthesized in the hybrid composite fashion through *in situ* procedures.

Spurred by this controversy, we prepared a series of hybrid composites where rGO in different amounts has been incorporated in a hierarchical zinc oxide scaffold. In order to separate the possible contributions in photocatalysis provided by rGO itself, we chose, unlike most investigations, to conformally and completely enwrapping rGO within the semiconductor, thus generating an *internal* heterojunction not exposed to the surrounding environment. This rare configuration allowed to investigate the actual effect of rGO on ZnO, selected as a model of catalytic semiconducting metal oxides, performance.

Moreover, we investigated the effects on the crystalline quality of the ZnO nanostructures due to the application of an *in situ* procedure to synthesize the GSHCs, supported by microwave heating, where the rGO sheets were exploited as platform for the uptake of Zn^{2+} ions (used as ZnO precursor). Obtained GSHCs were thus characterized and tested as photocatalysts, with the specific aim of shedding light on the relations between structure and performance.

2. Materials and Methods

2.1. Synthesis of materials.

Zinc acetate dihydrate (ACS reagent, ≥98%), reduced graphene oxide (carbon ≥75%, oxygen ≤22%), and hexamethylenetetramine (ACS reagent, ≥99%) were purchased from Sigma-Aldrich and used without any further treatment. Distilled H_2O and ethanol were used as solvents. Zinc oxide nanoparticles were synthesized based on a modified synthesis as that proposed by Wang and collaborators.[27] Briefly, rGO was added to a 0.01M aqueous solution of $Zn(CH_3COOH)_2 \cdot 2H_2O$ (0.01-10 wt% with respect to ZnO).

The suspension was stirred for 2 hours to allow the uptake of Zn^{2+} ions on the rGO sheets, after which hexamethylenetetramine (HMTA) was added in an equimolar ratio with respect to zinc acetate dihydrate. Ethanol was then added in a 1:9 volume ratio of H_2O:CH_3CH_2OH. The reaction mixture was heated in a microwave oven (Milestone flexiWAVE) at 500 W for 30 minutes, resulting in a suspension of ZnO particles, which was centrifuged and washed to recover a fine powder. The powder was then heat treated at 300 °C in air for 8 hours. Materials with rGO concentrations of 0, 0.01, 0.1, 0.5, 1.0, and 2.0 wt% were prepared.

2.2. Electrode preparation.

Electrodes for electrochemical characterization were prepared by suspending rGO-ZnO particles in a slurry, which was then spread on FTO-coated glass and heat treated. The slurry was made by adding 1.4 g/ml of polyethylene glycol to a 3:2:1 (volume) mixture of ethanol, α-terpineol, and water.

2.3. Characterization.

Diffuse reflectance and absorption spectra were recorded with an Agilent Cary5000 UV-Vis spectrophotometer using an integrating sphere. Photoluminescence was recorded using an FLS980 spectrofluorimeter from Edinburgh Instruments; steady state emission spectra were recorded using a xenon arc lamp as excitation source, time-resolved measurements were performed using time-correlated single photon counting (TCSPC) with a 371.8 nm pulsed diode laser as excitation source. X-ray patterns were recorded in Bragg-Brentano geometry with a PANalytical Empyrean diffractometer, operating at 45 kV and 40 mA, using a copper anode. SEM analysis was carried out with a FEI Magellan 400L. The structural analysis at the nanoscale was carried out on a

FEI Tecnai F20 high resolution transmission electron microscope (HR-TEM) operated at 200 kV. Electrochemical measurements were performed in a three-electrode configuration, using a platinum plate counter electrode and an Ag/AgCl reference electrode, on a ModuLab XM ECS potentiostat from Solartron Analytical in 1.0 M aqueous solution of Na_2SO_4, in a potential range from -1 to 0.6 V *vs.* Ag/AgCl. The electrochemical cells were purged with argon gas for 30 minutes to remove dissolved oxygen before measurement. Electrochemical impedance spectroscopy with an AC signal of 100 mV in amplitude, in the frequency range between 10 Hz and 1 MHz and an applied bias equal to the OCV of the system (200 mV).

2.4. Photocatalytic tests.

Photocatalytic performance of ZnO and rGO-ZnO samples were evaluated by measuring the degradation of 10^{-6} M rhodamine B (RhB) and 10^{-4} M phenol (PhOH) in water, both loaded with 0.5 g/l of catalyst, while under illumination. For the RhB degradation, the illumination was provided by a LOT-QD solar simulator, giving an AM1.5G spectrum at 1 sun intensity (calibrated with a silicon reference cell), while the PhOH solution was irradiated with UV light (6 W, 365 nm). The reaction course was followed by means of spectrophotometry, monitoring the absorption peak of rhodamine B centered at 554 nm and the absorption peak of phenol located at 270 nm.

3. Results and Discussion

3.1. Structural and morphological characterization

Hexamethylenetetramine was used in the synthetic mixture as a source of OH^- ions. This molecule is capable of supporting the formation of ZnO nanostructures, by slowly hydrolyzing, assuring a gradual release of hydroxyl ions in the synthetic mixture, which is particularly important when microwaves are used as heating sources, which speeds up the overall reaction rate,[28] thus promoting the formation of nanostructures.

ZnO synthesized structures are disc-shaped with porous surface and a relatively small size distribution, as shown by SEM analysis (Figure 1 a-d). The hexagonal symmetry of wurtzite ZnO is visible on the basal plane of the particles.

It is possible to notice the roughness of ZnO surfaces, more pronounced for the basal plane, due to microcracks. The formation of pores has been previously observed in case of ZnO structures generated via a hydrolytic process, [29] during which internal voids are naturally induced by the solvent penetration into deep areas of the intermediate reaction species. As mentioned before, there is some dispersion of particle sizes, but on average the particles have a diameter of approximately 1.5 µm, and a thickness of 500 nm, showing a hierarchical structure: significantly smaller particles can be identified, clustered together to give the microstructure. rGO addition with concentrations up to 1% does not result in any visible change in the ZnO microparticles morphology with respect to the pristine sample. Whereas the presence of rGO cannot be detected by SEM, HR-TEM analysis reveals the presence of rGO nanosheets protruding from ZnO microparticles in the composite featuring 1% rGO (Figure 1 d). The wrinkled structure of the nanosheets reveals the typical (0,0,2) and (1,1,0) reflections with d-spacing equal

to 0.34 nm and 0.21 nm, respectively. The 0.34 nm fringes correlated to graphene layer folding on itself: this is relevant information because, by counting the number of these fringes, it is possible to gain knowledge about the numbers of layers of the stacked structure, which in the present case were found to range between 10 and 20. However, it should be noted that this analysis could be done only for the 1% rGO composite, for which it was possible to observe the sheets, being the rGO, in all the other samples, conformally enwrapped by the ZnO structures.

The presence of rGO is also confirmed with Raman spectroscopy (Figure 2); all rGO-containing samples present a clear signal of rGO, i.e. the G- and D-bands at 1600 and 1350 cm^{-1} together with the E_2 low and high vibrational modes of ZnO. This finding indicates that ZnO must grow around the rGO sheets, resulting in a conformal coverage of these latter. The evaluation of I_D/I_G ratio in the composites shows values spanning from 0.67 to 0.79, far higher than the ratio reported for graphite (below 0.25), [30] thus reassuring about the presence of rGO in the materials under investigation (which might be put under question by the formation of multilayers, as evidenced by TEM analysis).

This has a significant relevance in terms of contact with the semiconducting MOx, which is considered a key feature for charge transport within the composites.[31] The conformal coverage of ZnO around rGO also strongly supports the hypothesis that *in situ* synthesis of such hybrid composites proceed through the uptake of Zn^{2+} ions on the C-materials prior to the reaction leading to the MOx.[32] Moreover, the conformal coverage of rGO sheets can result beneficial when testing the materials as photocatalysts: the rGO sheets will indeed be protected against reduction by the hydroxyl radicals possibly formed upon UV exposure of ZnO structures, as previously observed in literature.[6],[33] All the prepared materials show a hexagonal wurtzite

structure, as identified by XRD (reported in Figure S1 in the Supplementary Material) and HR-TEM analysis (Figure S2 in the Supplementary Material). Scherrer analysis confirms that the crystallite size is not affected by rGO addition (Figure S3 in the Supplementary Material), showing moreover a very good agreement with TEM analysis (Table S1 in the Supplementary Material). The absence of any peak ascribable to rGO in the X-ray diffractogram has been previously reported,[34][26] and in this case is attributed to the low concentration of rGO and the weak X-ray scattering power of carbon.

3.2. Photocatalytic degradation part (a): rhodamine B

All the materials are active photocatalysts featuring good performance in the degradation of rhodamine B: with or without rGO, near-complete discoloration of a 10^{-6} M aqueous solution of rhodamine B is obtained after 90 minutes of simulated sunlight illumination. The absorption spectrum of rhodamine B (Figure 3a) exhibits a hypsochromic shift in the later stages of the reaction. This is consistent with the N-deethylation of RhB to rhodamine, as previously reported[35], and no difference was observed for samples featuring different amounts of rGO, indicating that the presence of the carbon material does not change the reaction mechanism. The reaction course (Figure 3b) for the different materials shows a pseudo-first order reaction course, as also expected, and clearly indicates that rGO provides some benefit for the photocatalytic efficiency, especially for lower reaction times. Moreover, an interesting tendency of increased adsorption under dark is observed: from low to high rGO concentration, the adsorbed amounts are 12.5 (rGO content: 0.00%), 16.6 (rGO content: 0.01%), 17.6

(rGO content: 0.10%), 17.1 (rGO content: 0.50%), 18.7 (rGO content: 1.00%) and 23.0 (rGO content: 2.00%) nmol (the RhB uptake capability of bare rGO was found to equal to 15.3 nmol, shown in Figure S4 in the Supplementary Material). This effect has been observed before,[26][27] and it is usually attributed to dye adsorption by the rGO, especially due to a favorable π-π interaction between the core of the molecule and the carbon rings. However, in our materials the rGO sheets are preferentially enwrapped by the ZnO structures, which prevents a direct adsorption of dye molecules; moreover, the amount of adsorbed dye does not increase linearly with rGO content (see figure S5 in the Supplementary Material), as one would expect from a simple additive effect (although a more complex relationship could be expected from the wrinkling and stacking of sheets, as observed in Figure 1 d), so that other effects need to be considered. Previous investigations have reported a modified surface chemistry in P25-GO composites,[38] specifically a decrease in pH_{PZC} (point of zero charge) in the presence of GO. However, that effect likewise hinges on functional groups of GO/rGO being exposed to the adsorbate. It might therefore be surmised that the introduction of rGO into the synthesis increases the number of adsorption sites on the catalyst particles, which would in turn lead to an enhanced catalytic skill due to a proximity effect.

The benefit of rGO emerges more clearly from the analysis of the effective rate constants from the logarithmic concentration curves (Figure 3c, 3d), where it can be seen that the reaction rate monotonically increases with the rGO content in the composites up to 1 wt%. A concentration higher than 1% has however little effect and the curve is clearly reaching a plateau. As we mentioned, the optimal amount of carbon materials to be combined with semiconducting MOx for enhancing their functionality is

a controversial topic in literature and even detrimental effects of increasing the rGO loading has been observed before at similar concentrations. [8]

3.3. Photocatalytic degradation part (b): phenol

Phenol was tested as a non-absorbing substrate: indeed, photocatalytic data from RhB may provide a misrepresentation of the effect exerted by rGO on the catalytic skill of ZnO, due to photosensitization. All the materials under investigation were observed to be active photocatalysts also for the degradation of PhOH in water, as shown in the analysis of the catalytic process reported in Figure 4. Adsorption of the target pollutant on the composites did not show relevant differences ascribable to different rGO loadings (Figure 4 b). During the photocatalytic reaction, the intensity of PhOH absorption peak (centered at 270 nm) decreases and new spectral features appear, possibly ascribable to intermediates in the oxidative process that should eventually lead to CO_2 formation (Figure 4 a). The detailed identification of the reaction intermediates is beyond the scope of the present investigation, but, assuming the photodegradation mechanism involves hydroxyl radicals, as often reported in literature (a broad discussion about reactive oxygen species in semiconductor-supported photocatalysis can be found in reference [21]), we can hypothesize the presence of hydroquinones, quinones and catechol.

Bare ZnO appears more efficient at degrading the aromatic compound than any of the hybrid composites, as shown by the reaction course curves (Figure 4 b) and the apparent rate constant shows a clear decreasing trend with the presence of rGO within the catalyst (Figure 4 c). On the other hand, the reaction does not follow a pseudo-first

order kinetics: this is probably due to the concomitant presence in the reaction mixture of different species, which can as well undergo oxidative processes. A very similar result was reported by Minella and coworkers[39], who carried out the photocatalytic degradation of phenol with TiO_2/rGO composites: they also observed a decreased efficiency of the photocatalytic reaction upon the addition of rGO to TiO_2. The presence of rGO is not able to support the exciton lifetime, so to use the photogenerated charges to generate species active for PhOH oxidation, on the contrary, it is evident that these charges are either recombined more largely than without rGO or trapped in the composites.

Furthermore, it should be remarked that the differences in the adsorption of the target pollutants showed for RhB and PhOH can be related to the characteristics of the reaction mixtures and the catalysts. Indeed, the acidic character of both RhB (pKa = 4.2)[40] and phenol (pKa = 9.98)[41] should also be considered in this discussion: the reaction solutions featured a pH as high as 5.1 for RhB and 6.99 as for PhOH, in both cases lower than the pH_{PZC} of ZnO (reported to be between 7 and 9). [42–44] The PZC for rGO has been reported to be 3.5,[45] and, while combined with ZnO, graphene-derivatives materials have been proved to systematically lower the native pH_{PZC} of the MOx, [45–47] so that it is always lower than the pH of PhOH solution, while it can be higher or lower than the pH calculated for the RhB solutions, depending on the rGO amount incorporated in the composites. This in good agreement with the rather good adsorption capability featured by the composites towards RhB and their difficulty in uptaking the PhOH molecules.

3.3. Interaction with light: absorption and photoluminescence spectroscopic characterization

The light management inside the materials is one of the key parameters to consider, which we have investigated via UV-Vis spectroscopy (Figure 5) and photoluminescence spectroscopy (steady-state and time-resolved, Figure 6). The effect of rGO on the absorption properties is clear: increasing the rGO loading leads to an increased absorption in the visible range, while slightly reducing the absorbance in the UV-region. The decreased availability of UV light should lead to a reduction of catalytic efficiency of the ZnO, since for a wide band-gap semiconductor such as ZnO, it is the main source of energy for the catalytic reaction. However, it has been recently demonstrated that native ZnO defects permit some photoactivity even with visible light.[48]

We have previously reported on the significance of intrinsic crystalline defects in ZnO to photocatalytic performance in a similar material[49] and the application of photoluminescence spectroscopy to investigate them. Other groups have studied the relationship of native defects in ZnO with photocatalytic performance, with varying results.[50,51] Differences in outcome may be attributed to the location of defects – while surface defects can collect charges where they are available for reactions, charges trapped at bulk defect sites may not be useful. Another consideration is the type of defect and their charge state; this translates into different affinities for positive and negative charge carriers. It is therefore not trivial to state how defects affect the photocatalytic performance of a semiconductor, and in the present investigation we will limit the scope to observing the correlation of the intensity of defect-related luminescence with the functional performance of the material. The steady state and time-resolved photoluminescence data are reported in Figure 6. In the emission spectra,

the near-band-edge (NBE) band, located at 384 nm, and the visible band, peaking at approximately 650 nm, are apparent. The photoluminescence spectrum of ZnO has been extensively studied, and although the issue of assigning emissions to specific defects remains controversial,[52] it is widely agreed that the visible emissions originate from native defects in ZnO, such as vacancies and interstitials in the crystal structure. The more common green emission has usually been attributed to oxygen vacancies,[53] though this assignment has been challenged.[54] The origin of the red emission observed in our materials have not been conclusively identified.[55] It is worth pointing out that the emission wavelength of 650 nm is not a good match with any of the calculated energies of point defects in ZnO, and it could instead originate from complexes of different types of defects; however the energetics of defect complexes have not been extensively studied. The UV emission corresponds to direct recombination of photogenerated charge carriers and matches the band gap of ZnO. Overall, the introduction of rGO in the ZnO matrix has the effect of reducing the defect emissions, though the intensity ratio of UV to red emissions does not strictly correspond to the concentration of rGO. Moreover, there is a slight change in the shape of the visible band; while in the bare ZnO material there is a shoulder in the green part of the band, this is reduced or removed in the rGO-containing particles. This change in intensity, aside from a change in defect concentration, could possibly relate to the change in Fermi level that occurs in the junction between ZnO and rGO.

The time-resolved measurements reveal that there is a large difference in the lifetime of the two emission bands: the visible emissions are nearly 3 orders of magnitude slower than the NBE emissions in all samples. This is consistent with emission from defect-induced states[56] (the process is represented schematically in Figure 6d), where excited

electrons are captured by a shallow donor state provided by native defects in the material, then relax to the valence band or a deep acceptor state by emission of visible light. These states are localized around the defect and act as long-lived electron traps. The average lifetime of the NBE emission (Table 1) is slightly increased in the rGO-containing materials, indicating a reduced rate of transitions to the shallow defect states, corresponding to the reduced defect concentration inferred from the ratio of the UV and red PL intensities in Figure 6a. Assuming that the rGO only influences the crystallinity of the ZnO directly surrounding it, the variation in defect concentrations that is observed here would only relate to bulk defects, since the rGO is wrapped within ZnO. This in turn explains the increased performance in the materials with reduced defect concentration, as these defects would act to trap charge carriers in the interior of the particles.

This hypothesis is moreover confirmed by the comparative analysis of the NBE peaks (not normalized), reported in Figure S6 in the Supplementary Material. The presence of rGO does not quench this signal, but, instead, results in an increased intensity, associated to a better crystalline quality of ZnO in the hybrid composites. This finding is of particular interest in the field of functional applications of rGO hybrid composites. Indeed, a reduced intensity of the NBE in ZnO-based composites has been many times indicated as due to rGO (or other graphene derivatives): the radiative recombination of the photogenerated excitons would be inhibited by the rGO, which would catch the charges and make them available for useful reactions.[57][58][59][60] In the present investigation, instead, the presence of rGO has the benefit of improving the overall crystalline quality of the semiconducting metal oxide, thus spurring its catalytic skills.

This outcome was previously observed, even if more seldom than a quenching of NBE signal.[61,62]

It is also relevant to remark that we did not observe any quenching as for the NBE intensity (reported in Figure S6 in the Supplementary Material).

3.4. Charge storing and transfer within the composites: electrochemical characterization

To investigate the electrochemical properties of the materials, three-electrode cells were set up with FTO glass coated with the rGO-ZnO material as working electrodes. Cyclic voltammograms obtained at a scan rate of 50 mV/s are shown in Figure 7a. All the systems behave in an irreversible way: this is clearly shown by the absence of a reverse peak in the backward scan sweep, implying that the rate of electron transfer is insufficient to maintain the surface equilibrium. It is worth noting that cathodic peaks appear only in case of samples featuring a rGO amount as high as 1.0 and 2.0%, located at -0.52V and +0.08V for the 1% rGO sample and -0.52V and +0.16V for the 2% rGO sample. Bare ZnO presents a weak cathodic peak centered at around +0.2 V, but for all the other materials only a low intensity contribution, that can be classified as shoulders, can be seen. This suggests that the peaks identified for the 2% rGO sample pertain to reduction processes associated to rGO (most probably reduction of surface species). It is also interesting to remark that, by polarizing the materials far from the equilibrium, there is no monotonic trend as for the current density with the amount of rGO embedded in the materials. Moreover, polarization of bare ZnO is higher or equal to that of samples featuring the presence of rGO. This finding is relevant from different

viewpoints. First of all, there is no direct correlation between the electrical conductivity of the materials and the amount of rGO, i.e. rGO is not supporting the current flow through the composites. This implies that the enhancement in the photocatalytic performance as for the RhB degradation is not ascribable to a better charge transport (as also indirectly confirmed by the catalytic tests on PhOH) . It is important to remind herein that the electrical conductivity of graphene derivatives is regarded as the main factor behind the enhancement of functional performance of GSHCs. A very interesting study has previously demonstrated that the electrical conductivity of graphene-related materials can be significantly deteriorated in such composites, while their observed performance as photocatalysts is improved,[63] supporting the outcome shown in the present investigation.

To investigate deeper the electrochemical features of the composites, charge transfer resistance (R_{CT}) was analyzed by means of electrochemical impedance spectroscopy (EIS). EIS analysis (shown in Figure 7b and Table 2) shows that all the samples are well behaved electrochemical cells, where kinetic and diffusion control mechanism is in action (as also confirmed by the corresponding Bode plots, reported in Figure S7 of the Supplementary Material. They can all be modeled by a simple equivalent circuit (shown as the inset in Figure 7b), composed by a Randles cell with the addition of a Warburg impedance accounting for the behavior at low frequencies, where polarization due to a combination of kinetic and diffusion processes is considered.

Charge transfer resistance is only slightly reduced, compared to bare ZnO, by the presence of rGO. However, samples containing rGO between 0.01% and 1% feature about the same resistance, and the sample containing 2% rGO is the specimen with the lowest R_{ct} (values are reported in Table 2). This outcome further supports what

observed in the comparative analysis of CV measurements and photocatalysis results: it is not possible to claim a correlation between the charge transport characteristics featured by the hybrid composites with their capability of photodegrading organics in water.

It is also interesting to notice that, while at high frequencies all the samples behave in the same way, presenting a regular semicircle, at low frequencies the contribution coming from the diffusion process, and modeled by a Warburg impedance, is different. By considering only the rGO containing samples, the slope of this contribution shows a monotonic increase with increasing rGO amount, indicating a decreasing impedance. Lastly, the double-layer capacitance (C_{dl}) is increased by the addition of rGO; this might be the most significant indicator of a good photocatalyst, being directly related to the ability of the material to maintain sufficient charge on its surface to be useful for catalyzing reactions.

It is interesting to remark that in a previous work dealing with photoanodes for dye sensitized solar cells, where we synthesized hybrid graphene-TiO_2 composites to be exploited as electron transport materials,[64] we found a very similar result. While no significant differences were recorded among the composites as for recombination resistance (i.e. the skill of a material to sustain the life of the photogenerated exciton pairs), the key factor identified as the reason behind the enhanced performance was an increased chemical capacitance, which is in agreement to the outcomes shown in the present investigation for what concerns the transport of charges photogenerated on a photosensitizable substrate.

4. Conclusions

Zinc oxide benefits from the introduction of rGO in terms of photocatalytic performance as for the degradation of a visible absorber molecular target: the apparent rate constant is increased and the hybrid composites can degrade a (rather) higher amount of RhB. The increased efficiency is attributed to the increased rhodamine B adsorption, a reduced amount of crystalline defects, induced by the insertion of rGO in the synthetic mixture and the favorable electrochemical properties in the composite materials.

However, the most relevant role played by rGO seems to be that of supporting the synthesis of a ZnO hierarchical structure featuring better crystalline quality. The sustain provided by rGO in terms of enhanced charge transport, although evidenced by a reduction of the charge transfer resistance, appears to play a minor role. The gains of increasing rGO concentration taper off rapidly, possibly due the absorption of light by rGO. This strongly indicates that a balance must be identified between the relative amounts of the two partners, which possibly also depends on the aspect of ZnO. Furthermore, when a non-absorbing substrate is used as catalytic target, the mentioned benefits are no more useful, highlighting the role in catalysis played by proximity, adsorption of the molecular target on the catalyst and photosensitization. These outcomes underline that extreme care must be used when analyzing the catalytic performance of hybrid composites, which need a detailed consideration of all the possible factors involved in the catalytic process.

It should not be forgotten, when designing a hybrid catalyst, that the main player will still be the semiconductor, whose features can be properly enhanced and supported by the presence of rGO, through a material-by-design approach.

The present investigation highlights that a multi-parameters and detailed analysis of hybrid composites is needed, to consider as many factors as possible that are the reasons behind the observed enhancement of functional performance.

Declaration of Competing Interest

The authors declare that they have no known competing financial interests or personal relationships that could have appeared to influence the work reported in this paper.

Acknowledgements

The authors acknowledge the financial support from Knut & Alice Wallenberg foundation, Luleå University of Technology laboratory fund program, and Kempe foundation for partial funding. I.C. acknowledges VINNOVA under the VINNMER Marie cure incoming Grant for partial funding (project “Light Energy”, LiEN, 2015-01513). Carl Trygger Foundation is acknowledged for partial funding under the project “Water remediation through semiconductor-supported photocatalysis - WarCat”, Project No. CTS 19:70.

References

[1] G. Mamba, G. Gangashe, L. Moss, S. Hariganesh, S. Thakur, S. Vadivel, A.K. Mishra, G.D. Vilakati, V. Muthuraj, T.T.I. Nkambule, Journal of Environmental Chemical Engineering State of the art on the photocatalytic applications of graphene based nanostructures : From elimination of hazardous pollutants to disinfection and fuel generation, J. Environ. Chem. Eng. 8 (2020) 103505. https://doi.org/10.1016/j.jece.2019.103505.

[2] H. Zhang, G. Chen, D.W. Bahnemann, Photoelectrocatalytic materials for environmental applications, J. Mater. Chem. 19 (2009) 5089–5121. https://doi.org/10.1039/B821991E.

[3] Q. Kuang, X. Wang, Z. Jiang, Z. Xie, L. Zheng, High-energy-surface engineered metal oxide micro- and nanocrystallites and their applications, Acc. Chem. Res. 47 (2014) 308–318. https://doi.org/10.1021/ar400092x.

[4] M. Khan, M.N. Tahir, S.F. Adil, H.U. Khan, M.R.H. Siddiqui, A.A. Al-Warthan, W. Tremel, Graphene based metal and metal oxide nanocomposites: synthesis, properties and their applications, J. Mater. Chem. A. 3 (2015) 18753–18808. https://doi.org/10.1039/c5ta02240a.

[5] G. Williams, B. Seger, P. V Kamat, UV-Assisted Photocatalytic Reduction of Graphene Oxide, 2 (2008) 1487–1491.

[6] I. V. Lightcap, T.H. Kosel, P. V. Kamat, Anchoring semiconductor and metal nanoparticles on a two-dimensional catalyst mat. storing and shuttling electrons with reduced graphene oxide, Nano Lett. 10 (2010) 577–583. https://doi.org/10.1021/nl9035109.

[7] F.K. Meng, J.T. Li, S.K. Cushing, J. Bright, M.J. Zhi, J.D. Rowley, Z.L. Hong, a Manivannan, a D. Bristow, N.Q. Wu, Photocatalytic Water Oxidation by Hematite/Reduced Graphene Oxide Composites, Acs Catal. 3 (2013) 746–751. https://doi.org/Doi 10.1021/Cs300740e.

[8] T. Xu, L. Zhang, H. Cheng, Y. Zhu, Significantly enhanced photocatalytic performance of ZnO via graphene hybridization and the mechanism study, Appl. Catal. B Environ. 101 (2011) 382–387. https://doi.org/10.1016/j.apcatb.2010.10.007.

[9] B.N. Joshi, H. Yoon, S.H. Na, J.Y. Choi, S.S. Yoon, Enhanced photocatalytic performance of graphene-ZnO nanoplatelet composite thin films prepared by electrostatic spray deposition, Ceram. Int. 40 (2014) 3647–3654. https://doi.org/10.1016/j.ceramint.2013.09.060.

[10] Y. Leng, W. Wang, L. Zhang, F. Zabihi, Y. Zhao, Fabrication and photocatalytical enhancement of ZnO-graphene hybrid using a continuous solvothermal technique, J. Supercrit. Fluids. 91 (2014) 61–67. https://doi.org/10.1016/j.supflu.2014.04.012.

[11] B. Weng, M.Q. Yang, N. Zhang, Y.J. Xu, Toward the enhanced photoactivity and photostability of ZnO nanospheres via intimate surface coating with reduced graphene oxide, J. Mater. Chem. A. 2 (2014) 9380–9389. https://doi.org/10.1039/c4ta01077a.

[12] F. Wang, Y. Zhou, X. Pan, B. Lu, J. Huang, Z. Ye, Enhanced photocatalytic properties of ZnO nanorods by electrostatic self-assembly with reduced graphene oxide, Phys. Chem. Chem. Phys. 20 (2018) 6959–6969.

https://doi.org/10.1039/c7cp06909j.

[13] A.G. Abd-Elrahim, D.-M. Chun, Room-temperature deposition of ZnO-graphene nanocomposite hybrid photocatalysts for improved visible-light-driven degradation of methylene blue, Ceram. Int. (2021). https://doi.org/10.1016/j.ceramint.2021.01.142.

[14] A. Trapalis, N. Todorova, T. Giannakopoulou, N. Boukos, T. Speliotis, D. Dimotikali, J. Yu, TiO<inf>2</inf>/graphene composite photocatalysts for NOx removal: A comparison of surfactant-stabilized graphene and reduced graphene oxide, Appl. Catal. B Environ. 180 (2016) 637–647. https://doi.org/10.1016/j.apcatb.2015.07.009.

[15] Y.H. Ng, I. V. Lightcap, K. Goodwin, M. Matsumura, P. V. Kamat, To What Extent Do Graphene Scaffolds Improve the Photovoltaic and Photocatalytic Response of TiO2 Nanostructured Films?, J. Phys. Chem. Lett. 1 (2010) 2222–2227. https://doi.org/10.1021/jz100728z.

[16] H. Zhang, X. Lv, Y. Li, Y. Wang, J. Li, P25-graphene composite as a high performance photocatalyst (Functionalized graphene), ACS Nano. 4 (2010) 380–386. https://doi.org/10.1021/nn901221k.

[17] N. Serpone, D. Lawless, J. Disdier, J.M. Herrmann, Spectroscopic, Photoconductivity, and Photocatalytic Studies of TiO2 Colloids: Naked and with the Lattice Doped with Cr3+, Fe3+, and V5+ Cations, Langmuir. 10 (1994) 643–652. https://doi.org/10.1021/la00015a010.

[18] M.I. Litter, J.A. Navfo, Photocatalytic properties of iron-doped titania semiconductors, J. Photochem. Photobiol. A Chem. 98 (1996) 171–181.

[19] M. Anpo, H. Nakaya, S. Kodama, Y. Kubokawa, K. Domen, T. Onishi, Photocatalysis over binary metal oxides. Enhancement of the photocatalytic activity of titanium dioxide in titanium-silicon oxides, J. Phys. Chem. 90 (2005) 1633–1636. https://doi.org/10.1021/j100399a036.

[20] N. Zhang, Y.J. Xu, The endeavour to advance graphene-semiconductor composite-based photocatalysis, CrystEngComm. 18 (2015) 24–37. https://doi.org/10.1039/c5ce01712b.

[21] G. Solomon, M.G. Kohan, A. Landström, A. Vomiero, I. Concina, Semiconducting metal oxides empowered by graphene and its derivatives: Progresses and critical perspective on selected functional applications, J. Appl. Phys. 128 (2020). https://doi.org/10.1063/5.0021826.

[22] M.Q. Yang, N. Zhang, Y.J. Xu, Synthesis of fullerene-, carbon nanotube-, and graphene-TiO2 nanocomposite photocatalysts for selective oxidation: A comparative study, ACS Appl. Mater. Interfaces. 5 (2013) 1156–1164. https://doi.org/10.1021/am3029798.

[23] H.R. Pant, C.H. Park, P. Pokharel, L.D. Tijing, D.S. Lee, C.S. Kim, ZnO micro-flowers assembled on reduced graphene sheets with high photocatalytic activity for removal of pollutants, Powder Technol. 235 (2013) 853–858. https://doi.org/10.1016/j.powtec.2012.11.050.

[24] G. Williams, P. V. Kamat, Graphene-semiconductor nanocomposites: Excited-state interactions between ZnO nanoparticles and graphene oxide, Langmuir. 25 (2009) 13869–13873. https://doi.org/10.1021/la900905h.

[25] X. Liu, L. Pan, T. Lv, Z. Sun, Investigation of photocatalytic activities over ZnO-

TiO2-reduced graphene oxide composites synthesized via microwave-assisted reaction, J. Colloid Interface Sci. 394 (2013) 441–444. https://doi.org/10.1016/j.jcis.2012.11.047.

[26] F.S. Omar, H. Nay Ming, S.M. Hafiz, L.H. Ngee, Microwave synthesis of zinc oxide/reduced graphene oxide hybrid for adsorption-photocatalysis application, Int. J. Photoenergy. 2014 (2014). https://doi.org/10.1155/2014/176835.

[27] M. Wang, S.H. Hahn, J.S. Kim, J.S. Chung, E.J. Kim, K.K. Koo, Solvent-controlled crystallization of zinc oxide nano(micro)disks, J. Cryst. Growth. 310 (2008) 1213–1219. https://doi.org/10.1016/j.jcrysgro.2008.01.001.

[28] I. Bilecka, M. Niederberger, Microwave chemistry for inorganic nanomaterials synthesis, Nanoscale. 2 (2010) 1358–1374. https://doi.org/10.1039/b9nr00377k.

[29] H.B. Kim, D.W. Jeong, D.J. Jang, Morphology-tunable synthesis of ZnO microstructures under microwave irradiation: Formation mechanisms and photocatalytic activity, CrystEngComm. 18 (2016) 898–906. https://doi.org/10.1039/c5ce02334c.

[30] D. López-Díaz, M. López Holgado, J.L. García-Fierro, M.M. Velázquez, Evolution of the Raman Spectrum with the Chemical Composition of Graphene Oxide, J. Phys. Chem. C. 121 (2017) 20489–20497. https://doi.org/10.1021/acs.jpcc.7b06236.

[31] P. V. Kamat, Photoinduced transformations in semiconductor-metal nanocomposite assemblies, Pure Appl. Chem. 74 (2002) 1693–1706. https://doi.org/10.1351/pac200274091693.

[32] T.S. Sreeprasad, S.M. Maliyekkal, K.P. Lisha, T. Pradeep, Reduced graphene oxide-metal/metal oxide composites: Facile synthesis and application in water purification, J. Hazard. Mater. 186 (2011) 921–931. https://doi.org/10.1016/j.jhazmat.2010.11.100.

[33] O. Akhavan, Photocatalytic reduction of graphene oxides hybridized by ZnO nanoparticles in ethanol, Carbon N. Y. 49 (2011) 11–18. https://doi.org/10.1016/j.carbon.2010.08.030.

[34] J. Zhang, Z. Xiong, X.S. Zhao, Graphene-metal-oxide composites for the degradation of dyes under visible light irradiation, J. Mater. Chem. 21 (2011) 3634–3640. https://doi.org/10.1039/c0jm03827j.

[35] T. Watanabe, T. Takizawa, K. Honda, Photocatalysis through excitation of adsorbates. 1. Highly efficient N-deethylation of rhodamine B adsorbed to cadmium sulfide, J. Phys. Chem. 81 (1977) 1845–1851. https://doi.org/10.1021/j100534a012.

[36] X. Li, Q. Wang, Y. Zhao, W. Wu, J. Chen, H. Meng, Green synthesis and photo-catalytic performances for ZnO-reduced graphene oxide nanocomposites, J. Colloid Interface Sci. 411 (2013) 69–75. https://doi.org/10.1016/j.jcis.2013.08.050.

[37] M. Ahmad, E. Ahmed, Z.L. Hong, J.F. Xu, N.R. Khalid, A. Elhissi, W. Ahmed, A facile one-step approach to synthesizing ZnO/graphene composites for enhanced degradation of methylene blue under visible light, Appl. Surf. Sci. 274 (2013) 273–281. https://doi.org/10.1016/j.apsusc.2013.03.035.

[38] S. Morales-torres, L.M. Pastrana-martínez, J.L. Figueiredo, J.L. Faria, A.M.T.

Silva, Applied Surface Science Graphene oxide-P25 photocatalysts for degradation of diphenhydramine pharmaceutical and methyl orange dye, Appl. Surf. Sci. 275 (2013) 361–368. https://doi.org/10.1016/j.apsusc.2012.11.157.

[39] M. Minella, F. Sordello, C. Minero, Photocatalytic process in TiO2/graphene hybrid materials. Evidence of charge separation by electron transfer from reduced graphene oxide to TiO2, Catal. Today. 281 (2017) 29–37. https://doi.org/10.1016/j.cattod.2016.03.040.

[40] R. Zhang, M. Hummelgrd, G. Lv, H. Olin, Real time monitoring of the drug release of rhodamine B on graphene oxide, Carbon N. Y. 49 (2011) 1126–1132. https://doi.org/10.1016/j.carbon.2010.11.026.

[41] M.D. Liptak, K.C. Gross, P.G. Seybold, S. Feldgus, G.C. Shields, Absolute pKa determinations for substituted phenols, J. Am. Chem. Soc. 124 (2002) 6421–6427. https://doi.org/10.1021/ja012474j.

[42] K.A. Isai, V.S. Shrivastava, Photocatalytic degradation of methylene blue using ZnO and 2%Fe–ZnO semiconductor nanomaterials synthesized by sol–gel method: a comparative study, SN Appl. Sci. 1 (2019) 1–11. https://doi.org/10.1007/s42452-019-1279-5.

[43] H. Benhebal, M. Chaib, T. Salmon, J. Geens, A. Leonard, S.D. Lambert, M. Crine, B. Heinrichs, Photocatalytic degradation of phenol and benzoic acid using zinc oxide powders prepared by the sol-gel process, Alexandria Eng. J. 52 (2013) 517–523. https://doi.org/10.1016/j.aej.2013.04.005.

[44] N. Kataria, V.K. Garg, Optimization of Pb (II) and Cd (II) adsorption onto ZnO nanoflowers using central composite design: isotherms and kinetics modelling, J.

Mol. Liq. 271 (2018) 228–239. https://doi.org/10.1016/j.molliq.2018.08.135.

[45] B. Tatykayev, F. Donat, H. Alem, L. Balan, G. Medjahdi, B. Uralbekov, R. Schneider, Synthesis of core/shell ZnO/RGO nanoparticles by calcination of ZIF-8/RGO composites and their photocatalytic activity, ACS Omega. 2 (2017) 4946–4954. https://doi.org/10.1021/acsomega.7b00673.

[46] C. Rodríguez, C. Tapia, E. Leiva-Aravena, E. Leiva, Graphene oxide–zno nanocomposites for removal of aluminum and copper ions from acid mine drainage wastewater, Int. J. Environ. Res. Public Health. 17 (2020) 1–18. https://doi.org/10.3390/ijerph17186911.

[47] S. Archana, K.Y. Kumar, B.K. Jayanna, S. Olivera, A. Anand, M.K. Prashanth, H.B. Muralidhara, Versatile Graphene oxide decorated by star shaped Zinc oxide nanocomposites with superior adsorption capacity and antimicrobial activity, J. Sci. Adv. Mater. Devices. 3 (2018) 167–174. https://doi.org/10.1016/j.jsamd.2018.02.002.

[48] E. Cerrato, M.C. Paganini, E. Giamello, Photoactivity under visible light of defective ZnO investigated by EPR spectroscopy and photoluminescence, J. Photochem. Photobiol. A Chem. 397 (2020) 112531. https://doi.org/10.1016/j.jphotochem.2020.112531.

[49] A. Landström, A. V Soldatov, A. Vomiero, I. Concina, Thermal Defect Modulation and Functional Performance : A Case Study on ZnO – rGO Nanocomposites, 1900239 (2019) 1–6. https://doi.org/10.1002/pssb.201900239.

[50] J. Wang, P. Liu, X. Fu, Z. Li, W. Han, X. Wang, Relationship between oxygen defects and the photocatalytic property of zno nanocrystals in nafion membranes,

Langmuir. 25 (2009) 1218–1223. https://doi.org/10.1021/la803370z.

[51] D. Chen, Z. Wang, T. Ren, H. Ding, W. Yao, R. Zong, Y. Zhu, Influence of defects on the photocatalytic activity of ZnO, J. Phys. Chem. C. 118 (2014) 15300–15307. https://doi.org/10.1021/jp5033349.

[52] A.M.C. Ng, X.Y. Chen, A.B. Djuri, ZnO nanostructures for optoelectronics : Material properties and device applications, 34 (2010) 191–259. https://doi.org/10.1016/j.pquantelec.2010.04.001.

[53] M.Y. Guo, A.M.C. Ng, F. Liu, A.B. Djurîšić, W.K. Chan, H. Su, K.S. Wong, Effect of native defects on photocatalytic properties of ZnO, J. Phys. Chem. C. 115 (2011) 11095–11101. https://doi.org/10.1021/jp200926u.

[54] S. Hsieh, J. Ting, Applied Surface Science Characterization and photocatalytic performance of ternary Cu-doped ZnO / Graphene materials, Appl. Surf. Sci. 427 (2018) 465–475. https://doi.org/10.1016/j.apsusc.2017.06.176.

[55] A.B. Djurišić, Y.H. Leung, Optical properties of ZnO nanostructures, Small. 2 (2006) 944–961. https://doi.org/10.1002/smll.200600134.

[56] P. Rodnyi, I. Khodyuk, Optical and luminescence properties of zinc oxide (Review), Opt. Spectrosc. 111 (2011) 776–785. https://doi.org/10.1134/S0030400X11120216.

[57] X. Liu, L. Pan, Q. Zhao, T. Lv, G. Zhu, T. Chen, T. Lu, Z. Sun, C. Sun, UV-assisted photocatalytic synthesis of ZnO-reduced graphene oxide composites with enhanced photocatalytic activity in reduction of Cr(VI), Chem. Eng. J. 183 (2012) 238–243. https://doi.org/10.1016/j.cej.2011.12.068.

[58] F. Wang, Y. Zhou, X. Pan, B. Lu, J. Huang, Z. Ye, Enhanced photocatalytic properties of ZnO nanorods by electrostatic self-assembly with reduced graphene oxide, Phys. Chem. Chem. Phys. 20 (2018) 6959–6969. https://doi.org/10.1039/c7cp06909j.

[59] B. Xue, Y. Zou, Uniform distribution of ZnO nanoparticles on the surface of grpahene and its enhanced photocatalytic performance, Appl. Surf. Sci. 440 (2018) 1123–1129. https://doi.org/10.1016/j.apsusc.2018.01.299.

[60] K.S. Ranjith, P. Manivel, R.T. Rajendrakumar, T. Uyar, Multifunctional ZnO nanorod-reduced graphene oxide hybrids nanocomposites for effective water remediation: Effective sunlight driven degradation of organic dyes and rapid heavy metal adsorption, Chem. Eng. J. 325 (2017) 588–600. https://doi.org/10.1016/j.cej.2017.05.105.

[61] B. Panigrahy, D.D. Sarma, Enhanced photocatalytic efficiency of AuPd nanoalloy decorated ZnO-reduced graphene oxide nanocomposites, RSC Adv. 5 (2015) 8918–8928. https://doi.org/10.1039/c4ra13245a.

[62] R. Yadav, V. Kumar, V. Saxena, P. Singh, V.K. Singh, Preparation of controlled lotus like structured ZnO decorated reduced graphene oxide nanocomposites to obtain enhanced photocatalytic properties, Ceram. Int. 45 (2019) 24999–25009. https://doi.org/10.1016/j.ceramint.2019.04.142.

[63] B. Weng, Y.J. Xu, What if the Electrical Conductivity of Graphene Is Significantly Deteriorated for the Graphene-Semiconductor Composite-Based Photocatalysis?, ACS Appl. Mater. Interfaces. 7 (2015) 27948–27958. https://doi.org/10.1021/acsami.5b10298.

[64] K.T. Dembele, G.S. Selopal, R. Milan, C. Trudeau, D. Benetti, A. Soudi, M.M. Natile, G. Sberveglieri, S. Cloutier, I. Concina, F. Rosei, A. Vomiero, Graphene below the percolation threshold in TiO2 for dye-sensitized solar cells, J. Mater. Chem. A. 3 (2015) 2580–2588. https://doi.org/10.1039/c4ta04395b.

FIGURE CAPTIONS

Figure 1. (a-d): SEM micrographs of synthesized material without rGO (a) and (b), and with 0.1% rGO (c) and (d), scale bars: 500 nm; (e,f): high magnification TEM micrographs of rGO protruding from a particle (1% rGO). d-spacings equal to 0.34 nm and 0.21 were highlighted in the inset (d), corresponding to graphite (110) and (002) planes.

Figure 2. (a) Raman spectra of ZnO (bottom line) and rGO-ZnO composite with increasing rGO content from bottom to top. (b): zoomed view of D- and G-band region (bare ZnO excluded) for the composite materials (increasing rGO amount from bottom to top).

Figure 3. (a) Rhodamine B absorption spectra during a photocatalytic reaction; (b) rhodamine B concentration over time during reaction course; (c) logarithmic concentration curves; (d) effective rate constant as function of rGO content.

Figure 4. Phenol photocatalytic degradation: (a) absorption spectra; (b) phenol concentration over time; (c) apparent rate constant as function of rGO content.

Figure 5. Diffuse reflectance (a) and corresponding Kubelka-Munk functions (b) of

rGO-ZnO particles.

Figure 6. (a) Steady-state photoluminescence emission of all materials, normalized to NBE peak; time-resolved photoluminescence plots of (b) NBE and (c) visible emission bands of bare ZnO. Black dots are the measured data points, the black line in (b) is the instrument response function, and the red lines in (b) and (c) are the fitted functions. (d) Schematic representation of energy levels and photoluminescence emissions in the material: (1) direct recombination of conduction band electron; (2) transition to trap state; (3) deep-level emission (DLE) from trap state.

Figure 7. (a) Cyclic voltammograms and (b) Nyquist plot of ZnO and rGO-ZnO electrodes.

TABLES

Table 1. Mean lifetimes of near-band-edge and visible photoluminescence emissions.

RGO content (%)	NBE mean lifetime (ps)	VIS mean lifetime (ns)
0	67.0	53.7
0.01	79.0	44.6
0.10	67.0	54.5
0.50	84.5	43.6
1.00	79.7	48.3
2.00	89.2	46.3

Table 2. Electrochemical parameters retrieved from the fitting of EIS measurements.

rGO content (%)	R_s (Ω)	R_{ct} (Ω)	C_{dl} (nF)	Warburg diffusion slope
0	5.64	22.2	28.5	---
0.01	5.90	19.8	32.0	-1.89
0.10	5.44	20.6	38.7	-1.68
0.50	5.80	20.3	31.3	-1.56
1.00	5.53	20.5	30.9	-1.54
2.00	5.13	19.3	41.5	-1.18

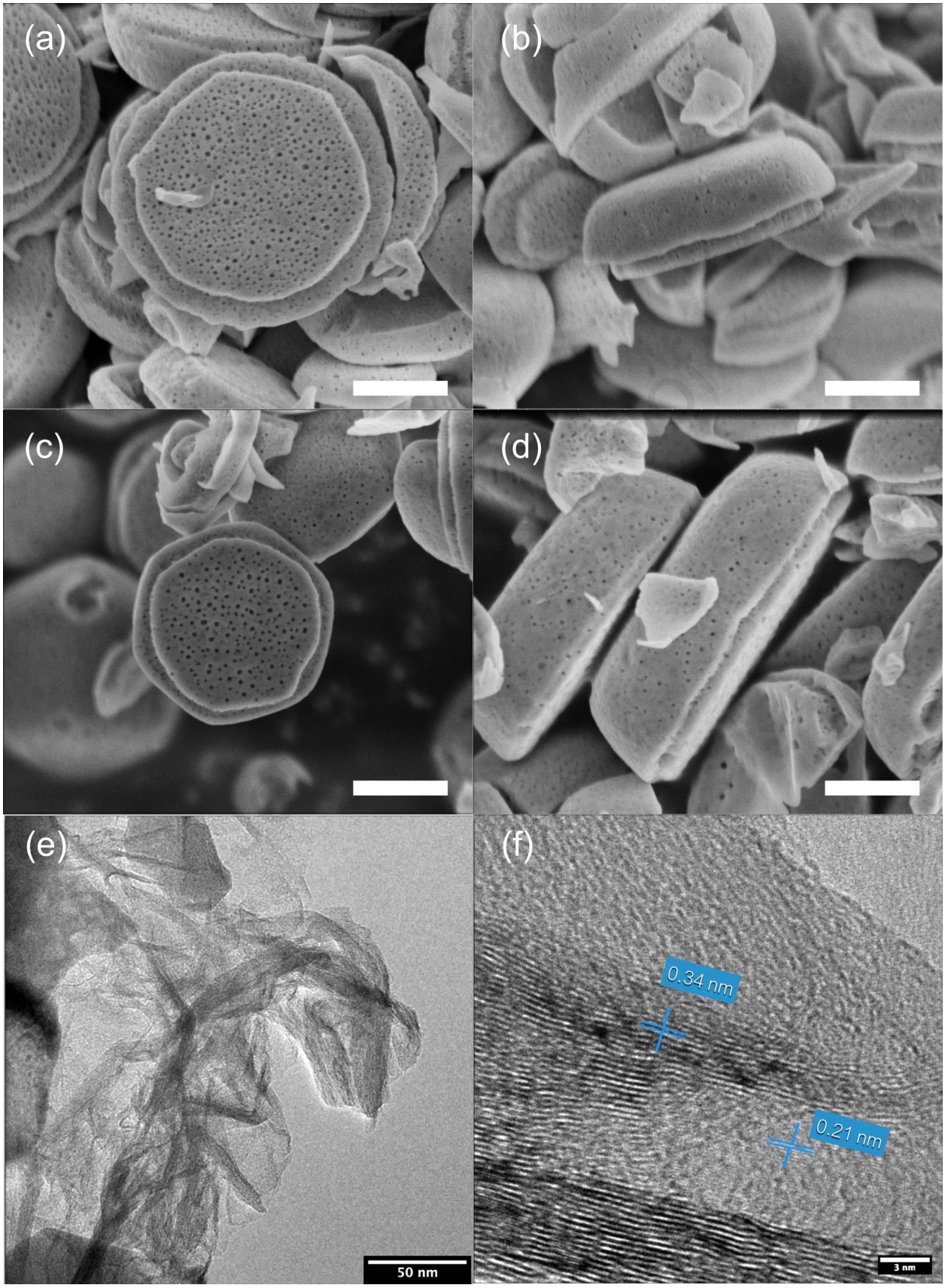
(a)
(b)
(c)
(d)
(e)
(f)
0.34 nm
0.21 nm
50 nm
3 nm

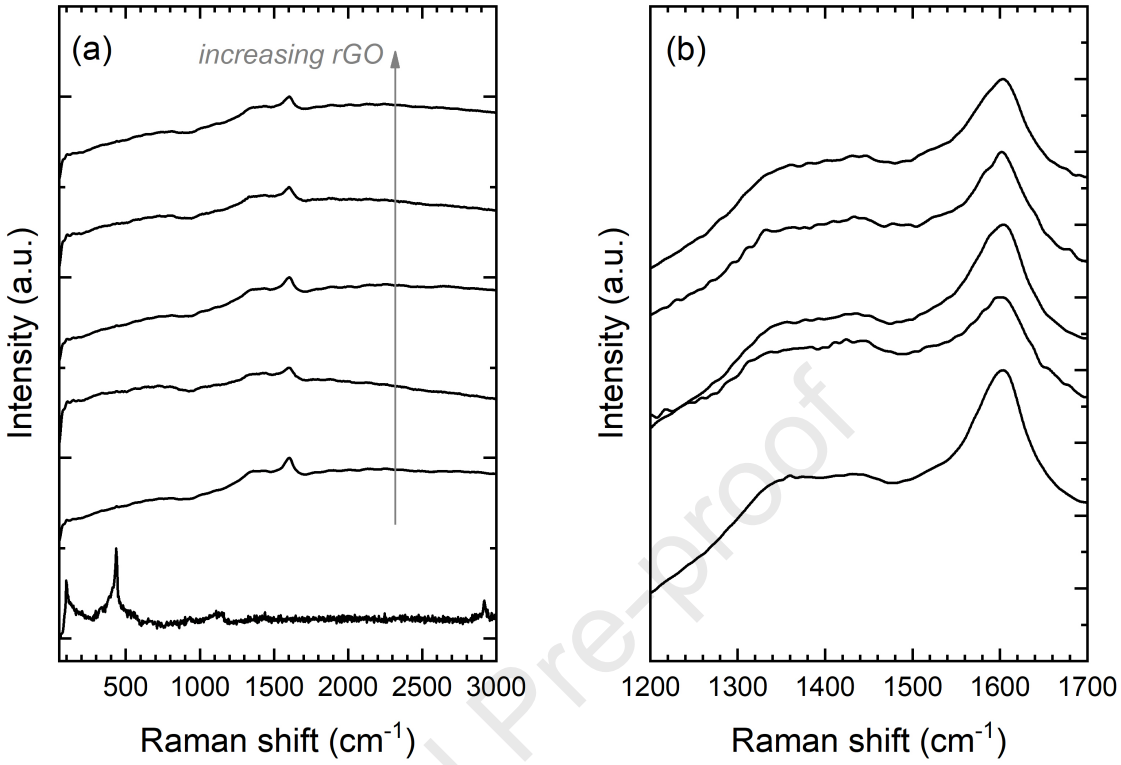

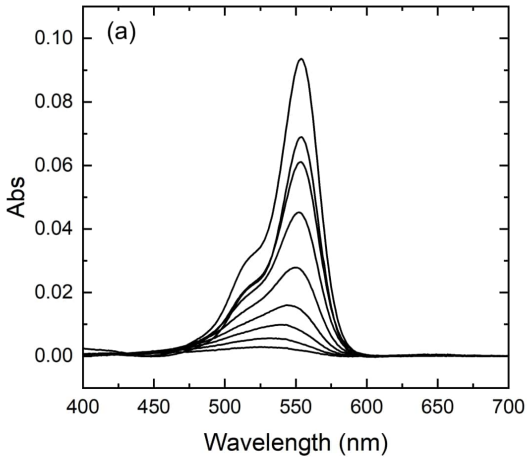

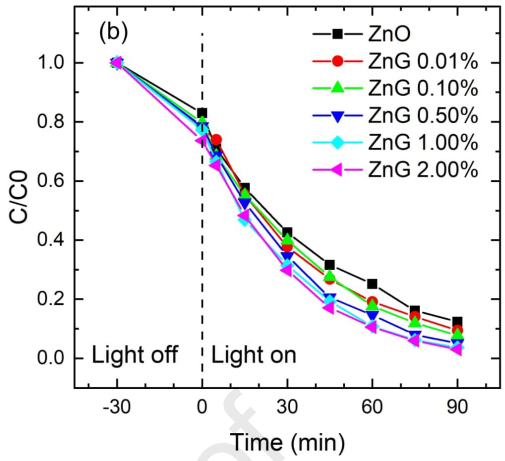

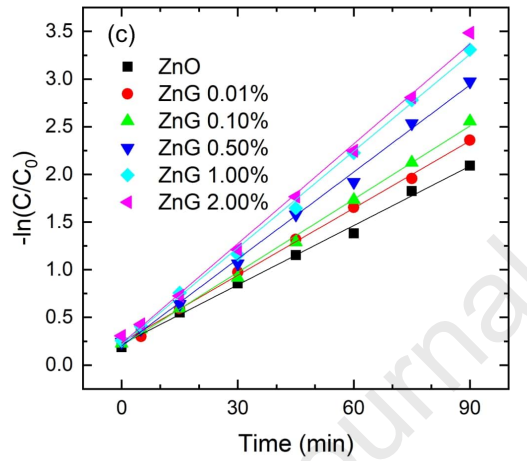

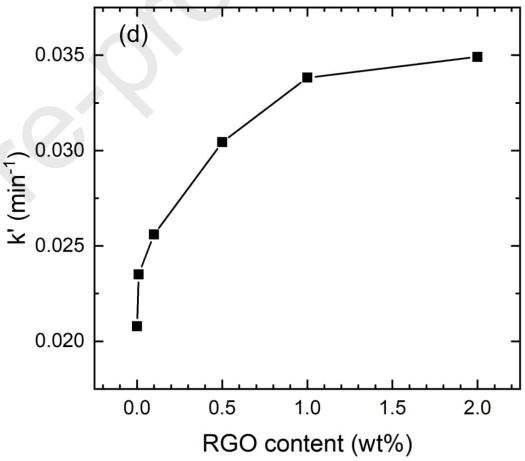

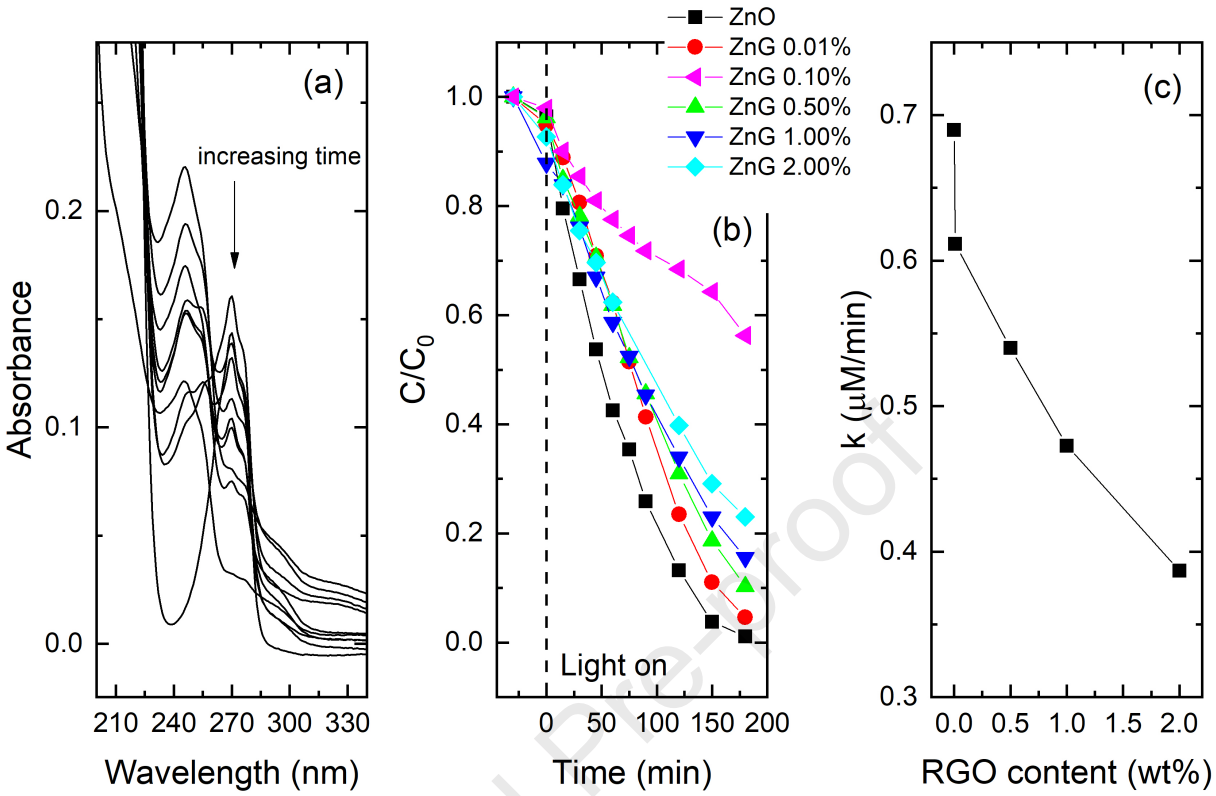

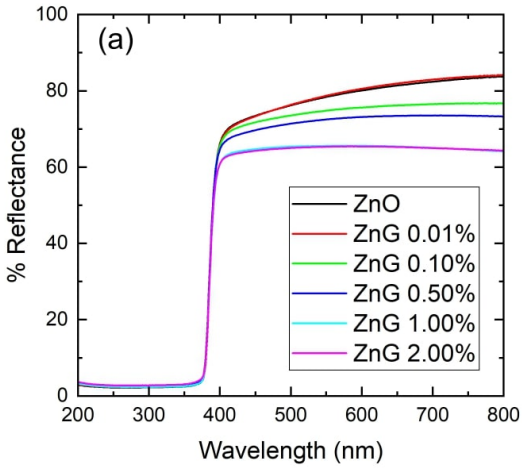

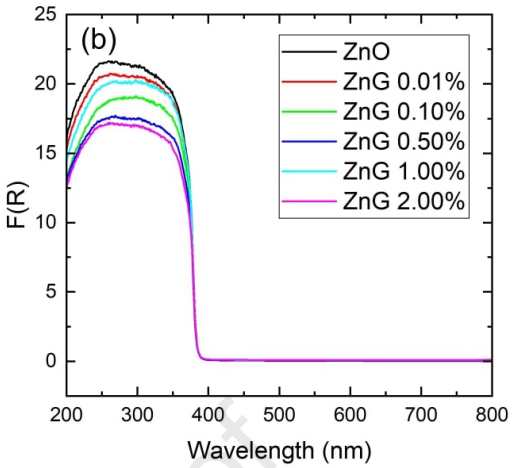

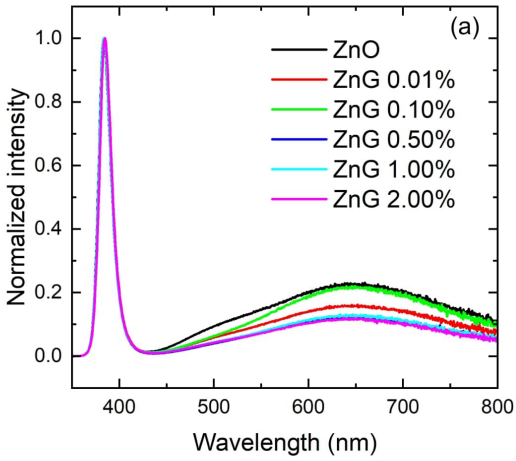

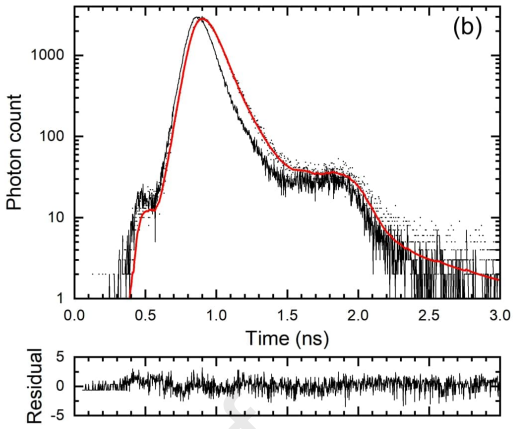

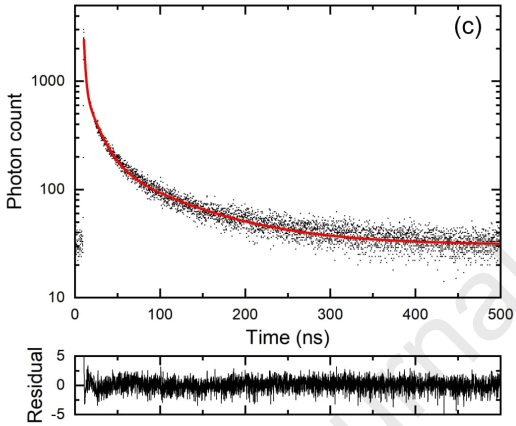

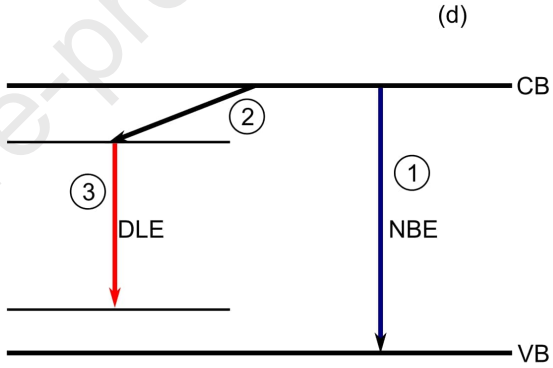

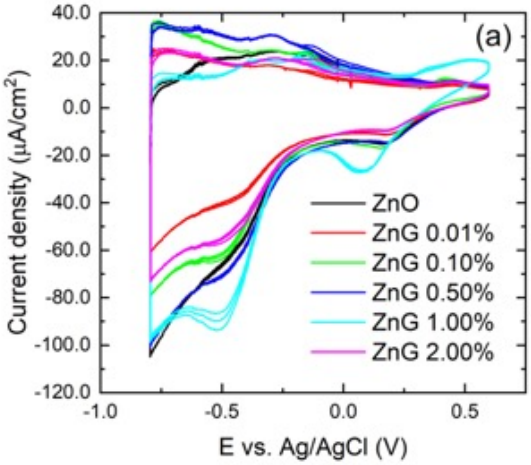

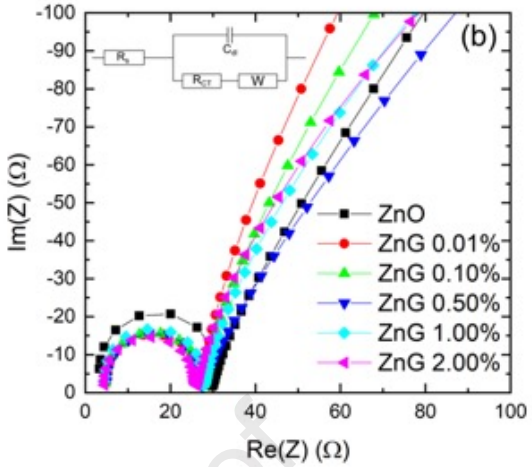

Declaration of interests

☒ The authors declare that they have no known competing financial interests or personal relationships that could have appeared to influence the work reported in this paper.

☐The authors declare the following financial interests/personal relationships which may be considered as potential competing interests: